Title: Single Gyroid and Inverse *b.c.c.* Photonic Crystals in Bird Feathers

Short title/running head: Avian Cubic Photonic Crystals

Field Codes: Materials Science and Evolutionary Biology

Authors:

Vinodkumar Saranathan[1-4, 7*], Suresh Narayanan[5], Alec Sandy[5], Eric R. Dufresne[6], and Richard O. Prum[7]

Affiliations:

[1]*Division of Science, Yale-NUS College, 10 College Avenue West, 138609, Singapore.*

[2]*NUS Nanoscience and Nanotechnology Initiative (NUSNNI-NanoCore), National University of Singapore, 117581, Singapore.*

[3]*Department of Biological Sciences, National University of Singapore, 117543, Singapore.*

[4]*Lee Kong Chian Natural History Museum, National University of Singapore, 117377, Singapore.*

[5]*Advanced Photon Source, Argonne National Laboratory, Lemont, Illinois, 60439, USA.*

[6]*Department of Materials Science, ETH, Zurich, Switzerland*

[7]*Department of Ecology and Evolutionary Biology, and Peabody Museum of Natural History, Yale University, New Haven, CT 06520, USA.*

*Correspondence to: Vinodkumar.Saranathan@aya.yale.edu

Abstract (124 words):

Vivid, saturated structural colors are a conspicuous and important aspect of the appearance of many organisms. A huge diversity of underlying 3D ordered biophotonic nanostructures has been documented, for instance, within the chitinaceous exoskeletons of insects. Here, we report diverse, highly ordered, intracellular, 3D biophotonic crystals in vivid plumages from three families of birds, which have each evolved independently from quasi-ordered (glassy) ancestral states. These morphologies include exotic bi-continuous single gyroid β-keratin and air networks, inverse *b.c.c.* and inverse opal (*r.h.c.p.*) close-packings of air spheres in the medullary β-keratin of feather barbs. These self-assembled avian biophotonic crystals may serve as biomimetic inspiration for advanced multi-functional applications, as they suggest alternative routes to the synthesis of optical-scale photonic crystals, including the experimentally elusive single gyroid.

One Sentence Summary: Evolutionary disorder-order transitions in bird feathers suggest direct optical scale self-assembly of photonic crystals

Main Text (1685 words; including references, notes and captions – 2857 words):

Organisms often use pigments to produce colors by wavelength-selective absorption of visible light(*1*). However, many organisms also produce vivid, saturated structural colors via constructive interference of light scattered from diverse integumentary nanostructures with mesoscopic (~100-350 nm) periodic or quasi-periodic order(*1, 2*). A rich diversity of structural color producing biophotonic nanostructures has been characterized, for instance, within the chitinaceous exoskeletons of invertebrates(*2, 3*). However, in vertebrates, structural colors are usually produced by well-characterized 1D (including thin-films, multi-

47 layers and diffraction gratings), and 2D biophotonic crystals, a prime example being the
48 ordered arrays of melanosomes in bird feather barbules(*2, 4*). Whereas, two classes of 3D,
49 quasi-ordered or glassy biophotonic nanostructures with short-range order are known to
50 generate non-iridescent or isotropic structural colors in feather barbs(*4, 5*). Organismal
51 structural colors are abundant in nature and constitute a key part of the animal appearance as
52 they are often used in sexual signaling, aposematism, and crypsis(*6*). Biophotonic
53 nanostructures are also receiving growing attention from physicists and engineers towards the
54 bio-mimetic inspiration of novel multi-functional technologies(*7-9*, *10*).

55 Here, we investigate the biophotonic nanostructures present within highly iridescent
56 and/or glossy feather barbs of Blue-winged Leafbird (*Chloropsis cochinchinensis*,
57 Chloropseidae), six species of *Tangara* tanagers (Thraupidae), and Opal-crowned Manakin
58 (*Lepidothrix iris*, Pipridae) using synchrotron small angle X-ray scattering (SAXS), scanning
59 (SEM) and transmission electron microscopy (TEM). We compare them to homologous
60 nanostructures of their close, evolutionary relatives(*5*), and identify at least three independent
61 evolutionary origins of 3D biophotonic crystals, including the elusive single gyroid, from
62 ancestral glassy nanostructural states in these three clades of tropical frugivorous perching
63 birds.

64 SEM images of feather barbs of *C. cochinchinensis*, reveal highly ordered
65 interconnected mesoporous networks of β-keratin rods with a polycrystalline texture (Figs.
66 1b, c, and S1d-f), while those of some *Tangara* species (Figs. 1g, h, and S1j-l; see Table S1)
67 and opal crown of *L. iris* (Figs. S1x-z) reveal highly ordered, close-packed arrays of air
68 spheres in the β-keratin matrix of medullary cells.

69 The SAXS diffraction patterns of feather barbs of *C. cochinchinensis* generally
70 exhibit six-fold symmetry and up to 8 orders of discrete Bragg spots (Figs. 1d, 3a, and b)
71 diagnosable as single gyroid ($I4_132$) space group (See Supplementary Results). The SAXS

patterns from feather barbs of six *Tangara* tanagers (Table S1) exhibit liquid-like features (Debye-Scherrer rings) together with discrete Bragg spots suggesting the presence of coexisting liquid and limited crystalline order, consistent with EM images (see Figs. 1i, and S1m-r). The corresponding azimuthal averages of the SAXS patterns (Figs. 1j, and S3b) reveal up to 7 orders of Bragg peaks diagnosable as body-centered cubic (*b.c.c.*; *Im*-3*m*) symmetry (see Supplementary Results). The *L. iris* crown feather barbs exhibit local face-centered cubic (*f.c.c.*) and hexagonal close-pack (*h.c.p.*) order, but overall the inverse opal nanostructure converges on random hexagonal close-pack (*r.h.c.p.*) symmetry as seen in many colloidal systems (see Supplementary Results).

The sister group to the *Chloropsis* leafbirds are fairy bluebirds (*Irena spp.*, Irenidae), which produce their structural blue barb colors using *channel*-type nanostructures (quasi-ordered interconnected mesoporous networks of β-keratin and air) with short-range order(*5*) (Figs. S1a-c). The feather structural colors of *Tangara* tanagers (Figs. S1g-i), and *Lepidothrix* manakins (Figs. S1s-u) are produced by *sphere*-type nanostructures (quasi-ordered arrays of air spheres in a β-keratin matrix), also with short-range order(*5*).

In order to gain insight into the evolutionary transitions from disorder-to-order in barb biophotonic nanostructures, we plot the coherence length ($\xi \approx 2\pi/\Delta q$, where Δq is the FWHM of the structural correlation peak), a measure of the long range periodic order (*i.e.*, approximate crystallite domain sizes) against the corresponding structural correlation peaks (q_{pk}) for both ordered and quasi-ordered barb nanostructures on *Ashby* diagrams (Figs. 2, and S2), with the materials selection parameter of interest being the structural Q factor ($q_{pk}/\Delta q$). The distribution of quasi-ordered *channel*- and *sphere*-type nanostructures within *Irena*, *Tangara*, and *Lepidothrix* closely parallel each other and the structural Q factor isolines (Fig. 2), suggesting the presence of size- or scale-independent physical mechanisms*(11)* leading to the final self-assembled nanostructural states within each genus(*12, 13*). The phylogenetically

independent nanostructural transitions from quasi-order to order within *Chloropsis*, *Tangara*, and *Lepidothrix* are evident as distinct deviations from the scale-independent trend of their closest relatives, arising from a sharpening of the structural correlation peaks (Fig. 2; see Supplementary Results).

Interestingly, the diversity of barb nanostructures in *Chloropsis* (green line) exhibit a continuum of intermediate states (green triangles) from the ancestral *channel*-type nanostructures of *Irena* (blue dashed line) to the derived single gyroids of *C. cochinchinensis* (green asterisks; Figs. 2a, 3 and S3a). The coherence lengths of leafbird nanostructures increases with each additional higher-order peak observed in the corresponding azimuthal SAXS data (Fig. 3f). Whereas the barb nanostructures of *Irena* lie parallel to the Q = 4.0 isoline, those of *Chloropsis* are distributed on a slope that diverges significantly from that of *Irena* (Fig. 2a). On one end, we have two species of *Chloropsis* (*palawanensis* and *flavipennis*) with similar structural parameters to the ancestral barbs in *Irena* (Figs. 2a, 3e' and S3a). However, the azimuthal SAXS profiles of most of the transitional *Chloropsis* nanostructures clearly exhibit 1 to 2 additional higher-order peaks besides the second-order feature that is a usual characteristic of *channel*-type nanostructures(*5*) (Figs. 2a, 3c', d', and S3a). Finally, the single gyroids of *C. cochinchinensis* are clustered at upper end of this distribution (Fig. 2a).

The variation in nanostructures among *Chloropsis* species not only document the gradual evolutionary transition from disorder-to-order within the genus, but also provide evolutionarily time-frozen snapshots of the development of single gyroid from quasi-ordered mesoporous networks (*cf.* (*14*)). The higher-order peaks in these intermediate nanostructures have ratios close to √6-√8, √14, and √22-√24 and not √4 (Figs. 3c', d' and S3a), *i.e.*, close to a 2D hexagonal (*p6m*) symmetry (1:√3:√4:√7:√11:√12). This implies that the transition likely proceeds via intermediate phases with the nucleation of local nematic- or even hexatic-like

order (Figs. 3a"-e"), as opposed to an intermediate with *b.c.c.* symmetry. This finding is reminiscent of the well-studied 2D hexagonal columnar to double gyroid epitaxial transitions seen in block copolymers(*15, 16*). Such local, partially ordered domains are likely very small and isolated given the isotropic scattering profiles of the intermediates (Figs. 3c and d).

Inverse cubic close-packed biophotonic crystals in feather barbs have comparable coherence lengths to synthetic inverse opals self-assembled at avian-visible length scales (for *e.g.*, (*17*)) (Figs. 2b, S2b, and Table S1). Because there are no self-assembled, synthetic meso-scale single gyroids for comparison to those in leafbirds (reviewed in *18*), we plot those fabricated using lithographic techniques (Fig. 2, S2, and Table S1). However, single gyroid biophotonic crystals comprised of chitin networks in air are known to be present in the iridescent scales of certain butterfly wings(*19*) and weevil elytra(*3*). Butterfly (3.2 ± 0.5 μm) and weevil (3.5 ± 0.3) single gyroids on average exhibit >1.5x the coherence lengths of avian (1.9 ± 0.1 μm) or lithographic (2.1 ± 0.4 μm) single gyroids (Figs. 2a, and Table S1).

Single gyroid β-keratin and air biophotonic crystal networks that occur in feather barbs of *C. cochinchinensis* are derived from the quasi-ordered *channel*-type nanostructure that first evolved in the common ancestor of *Irena* and *Chloropsis*(*5, 20*). The inverse *b.c.c.* and inverse opal biophotonic crystals respectively in *Tangara spp.* (Table S1) and *L. iris* feathers are derived from ancestral quasi-ordered *sphere*-type nanostructures in close relatives(*5*), with likely multiple independent evolutionary origins within *Tangara*(*21*). These origins of 3D photonic crystals documented here in feather barbs are evolutionarily parallel with the derivation of 2D hexagonal columnar biophotonic crystals in *Philepitta* from the primitive 2D quasi-ordered arrays of parallel collagen fibers in structurally colored skin of the most recent common ancestor with *Neodrepanis*, in Malagasy broadbills (Eurylaimidae)(*22*). In all four families, the evolutionary transitions to ordered biophotonic crystals with much narrower structural correlation peaks (see Figs. 6 and 7 of *22*, and Figs. 3,

147 S3, and S4) result in the production of more saturated or purer hues that are readily
148 perceivable by avian visual systems(*6*). These results suggest social or sexual selection on the
149 perceivable optical properties of biophotonic nanostructures – specifically, preferences for
150 purer, more saturated hues – have driven transitions in nanostructural spatial organization,
151 resulting in the evolution of extraordinarily brilliant structural coloration(*22, 23*).

152 Single gyroids have long been a target for photonic and photovoltaic engineering(*9,*
153 *10, 18*) due to their superior optical and electronic properties (large complete bandgaps), but
154 their self-assembly has been elusive, particularly at visible lengthscales (Fig. S2a). In insect
155 wing scales, single gyroid biophotonic crystals are templated by the co-option of the innate
156 ability of cell membranes to invaginate into core-shell double-gyroid precursor networks(*3,*
157 *13, 19, 24*). Extracellular chitin polymerizes within the space enclosed by the plasma
158 membrane and leaves behind a single gyroid network of chitin in air, upon apoptosis. Current
159 synthetic approaches to self-assemble single gyroids follow a similar pathway, starting with a
160 double gyroid or an alternating gyroid (*15, 18*) in a di- or tri-block copolymer and subsequent
161 selective etching of the matrix and one of the two network phases. Synthetic single gyroids
162 produced this way are limited to small lattice parameters (typically < 100 nm; Fig. S2a).
163 Synthetic lipid water systems also show cubic phases including double gyroid but with lattice
164 parameters limited to just tens of nm (*25*).

165 Glassy *channel*- and *sphere*-type biophotonic nanostructures of avian feather barbs
166 are understood to self-assemble within medullary cells via self-arrested, visco-elastic phase
167 separation of polymerizing β-keratin from the cytoplasm of the cell(*5, 26*). These
168 mechanisms are supported by the lack of any templating or prepatterning by cytoskeletal
169 components or cell membranes during the development of structurally colored barbs in
170 maturing feather germs(*12*). Our findings suggest that single gyroid (reviewed in *18*), inverse
171 opal and inverse *b.c.c.* photonic crystals may be conveniently and directly synthesized at

optical length scales through processes akin to bottom-up phase-separation. Simulations(*27*) suggest one possible route to self-assembling metastable single gyroid phases may involve patchy particles with mutual short-range attraction and long-range repulsion. Further research into *in vivo* and *in vitro* arrested phase separation of colloidal solutions of charged proteins or biosimilar polymers may provide novel biomimetic insights into synthetic self-assembly of ordered mesoporous single network structures for use in improved catalysis, photonics, or energy harvesting.

References and Notes:

1. D. L. Fox, *Animal Biochromes and Structural Colors*. (Univ. California Press, Berkeley, CA, 1976).
2. P. Vukusic, J. R. Sambles, Photonic structures in biology. *Nature* **424**, 852-855 (2003).
3. V. Saranathan *et al.*, Structural Diversity of Arthropod Biophotonic Nanostructures Spans Amphiphilic Phase-Space. *Nano Lett* **15**, 3735-3742 (2015).
4. R. O. Prum, in *Bird Coloration, Volume 1 Mechanisms and Measurements,* G. E. Hill, K. J. McGraw, Eds. (Harvard University Press, Cambridge, MA, 2006), vol. 1, pp. 295-353.
5. V. Saranathan *et al.*, Structure and Optical Function of Amorphous Photonic Nanostructures from Avian Feather Barbs: A Comparative Small Angle X-ray Scattering (SAXS) Analysis of 230 Bird Species. *Journal of The Royal Society Interface* **9**, 2563–2580 (2012).
6. I. C. Cuthill *et al.*, The biology of color. *Science* **357**, eaan0221 (2017).
7. M. Kolle *et al.*, Mimicking the colourful wing scale structure of the Papilio blumei butterfly. *Nat Nanotechnol* **5**, 511-515 (2010).
8. R. A. Potyrailo *et al.*, Morpho butterfly wing scales demonstrate highly selective vapour response. *Nat Photon* **1**, 123-128 (2007).
9. M. Saba *et al.*, Circular dichroism in biological photonic crystals and cubic chiral nets. *Physical Review Letters* **106**, 103902 (2011).
10. R. H. Siddique *et al.*, Bioinspired phase-separated disordered nanostructures for thin photovoltaic absorbers. *Science Advances* **3**, e1700232 (2017).

11. P. Fratzl, J. L. Lebowitz, O. Penrose, J. Amar, Scaling functions, self-similarity, and the morphology of phase-separating systems. Physical Review B 44, 4794-4811 (1991).

12. R. O. Prum, E. R. Dufresne, T. Quinn, K. Waters, Development of colour-producing β-keratin nanostructures in avian feather barbs. *Journal of The Royal Society Interface* **6**, S253-S265 (2009).

13. A. J. Parnell *et al.*, Spatially modulated structural colour in bird feathers. *Scientific reports* **5**, 18317 (2015).

14. B. D. Wilts *et al.*, Butterfly gyroid nanostructures as a time-frozen glimpse of intracellular membrane development. *Sci Adv* **3**, e1603119 (2017).

15. E. L. Thomas, MATERIALS SCIENCE:Enhanced: The ABCs of Self-Assembly. *Science* **286**, 1307- (1999).

16. M. F. Schulz, F. S. Bates, K. Almdal, K. Mortensen, Epitaxial Relationship for Hexagonal-to-Cubic Phase Transition in a Book Copolymer Mixture. *Physical Review Letters* **73**, 86-89 (1994).

17. B. Hatton, L. Mishchenko, S. Davis, K. H. Sandhage, J. Aizenberg, Assembly of large-area, highly ordered, crack-free inverse opal films. *Proc Natl Acad Sci U S A* **107**, 10354-10359 (2010).

18. J. A. Dolan *et al.*, Optical Properties of Gyroid Structured Materials: From Photonic Crystals to Metamaterials. *Advanced Optical Materials* **3**, 12-32 (2015).

19. V. Saranathan *et al.*, Structure, function, and self-assembly of single network gyroid (I4(1)32) photonic crystals in butterfly wing scales. *P Natl Acad Sci Usa* **107**, 11676-11681 (2010).

20. M. Moltesen, M. Irestedt, J. Fjeldsa, P. G. Ericson, K. A. Jonsson, Molecular phylogeny of Chloropseidae and Irenidae - cryptic species and biogeography. *Mol Phylogenet Evol* **65**, 903-914 (2012).

21. K. Burns, Molecular phylogenetics and biogeography of neotropical tanagers in the genus tangara. *Molecular Phylogenetics and Evolution* **32**, 838-854 (2004).

22. R. O. Prum, R. H. Torres, C. Kovach, S. Williamson, S. M. Goodman, Coherent light scattering by nanostructured collagen arrays in the caruncles of the Malagasy asities (Eurylaimidae: Aves). *Journal of Experimental Biology* **202**, 3507-3522 (1999).

23. R. O. Prum, Phylogenetic Analysis of the Evolution of Display Behavior in the Neotropical Manakins (Aves, Pipridae). *Ethology* **84**, 202-231 (1990).

24. Z. A. Almsherqi, S. D. Kohlwein, Y. Deng, Cubic membranes: a legend beyond the Flatland* of cell membrane organization. *Journal of Cell Biology* **173**, 839-844 (2006).

25. V. Luzzati, P. A. Spegt, Polymorphism of Lipids. *Nature* **215**, 701-704 (1967).

26. E. R. Dufresne *et al.*, Self-assembly of amorphous biophotonic nanostructures by phase separation. *Soft Matter* **5**, 1792-1795 (2009).

27. D. Stopper, R. Roth, Phase behavior and bulk structural properties of a microphase former with anisotropic competing interactions: A density functional theory study. *Phys Rev E* **96**, 042607 (2017).

Acknowledgments: We thank the ornithology curators and staff of the American Museum of Natural History in New York, the Museu Paraense Emílio Goeldi in Belem, Brazil, Museum für Naturkunde in Berlin, Germany, the University of Kansas Natural History Museum in Lawrence in Kansas, Yale Peabody Museum in New Haven, Connecticut, and the Lee Kong Chian Museum of Natural History in Singapore for loans and/or access to specimens examined in this research. TEM was done by Tim Quinn. Zhenting Zhang and Michael Rooks assisted with SEM. We thank Hui Cao and Heeso Noh for obtaining the thin paraffin sections of *L. iris* barbs. V.S. gratefully acknowledges Dan Morse and the Institute for Collaborative Biotechnologies at UCSB for support during a sabbatical that enabled some SAXS data collection. **Funding:** This work was supported with a Singapore NRF CRP Award (CRP20-2017-0004), Yale-NUS startup funds, a Royal Society Newton Fellowship and a Linacre College EPA Cephalosporin Junior Research Fellowship to V.S.; and Yale University W. R. Coe Funds to R.O.P. SAXS data collection at 8-ID, Advanced Photon Source, Argonne National Labs, was supported by the US Department of Energy, Office of Science, Office of Basic Energy Sciences, under Contract DE-AC02-06CH11357. **Author Contributions:** V.S. and R.O.P. designed the study. V.S., S.N., and A.S. performed SAXS measurements and VS analyzed the results. All authors discussed the data and results. V.S. wrote the manuscript, with input from R.O.P. and E.R.D. **Competing interests:** Authors declare no competing interests. **Data and availability:** All data is available in the main text or the supplementary materials.

Figure 1. Morphology of feather barbs with 3D biophotonic crystals. **Left panel** – Photographs, electron micrographs, and indexed 2D SAXS patterns in false color encoding of (**a-c**) iridescent blue epaulette, (**d**) green back of Blue-winged Leafbird (*Chloropsis c. cochinchinensis*, Chloropsidae); (**f**, **g**) yellow collar of Green-headed Tanager (*Tangara seledon*, Thraupidae); (**h**) bronze ear of Golden-eared Tanager (*T. chrysotis*); (**i**) shining green crown of Emerald Tanager (*T. f. florida*). **Right panel** – Structural diagnoses of Porod background corrected, azimuthally-averaged SAXS profiles of (**e**) iridescent blue scapular (turquoise line) of *C. cochinchinensis*, and (**j**) shining yellow nape (yellow line) of *T. florida*. The azimuthal SAXS profiles of ordered barbs are shown juxtaposed with those of quasi-ordered barbs in close relatives: (**e**) royal blue back (dark blue line) of Asian Fairy Bluebird (*Irena puella*, Irenidae) and (**j**) brassy shoulder (orange line) of Blue-necked Tanager (*T. cyanicollis*). Vertical lines denote expected Bragg peak positional ratios for *b.c.c.*(*Im*-3*m*), and single gyroid ($I4_132$). Scale Bars: EM images - 500 nm; SAXS patterns - 0.05 nm^{-1}. Abbreviations: **c** – cortex; **n** – necks. Photo credits (images cropped): (**a**) © Daniel J. Field, and (**f**) Lars Falkdalen Lindahl (CC BY-SA 3.0).

Figure 2. *Ashby* scatterplots highlighting evolutionary disorder-order transitions in (**a**) *channel*- and (**b**) *sphere*-type feather barb biophotonic nanostructures. The materials selection parameter of interest is the structural *Q*-factor ($q_{pk}/\Delta q$), plotted (dashed gray lines) as isolines in equally spaced deci-decades. Colored lines are linear regressions of log-transformed data in (**a**) for *Irena* fairy bluebirds (dashed blue), and *Chloropsis* leafbirds (green); and (**b**) inverse *b.c.c.* (green) and quasi-ordered *sphere*-type nanostructures of *Tangara* tanagers (dashed green), and *Lepidothrix* manakins (dashed blue). * denote single gyroid, ■ inverse *b.c.c.*, ⬢ inverse opal, while ▲ and ○ respectively denote quasi-ordered *channel*- and *sphere*-type nanostructures. For comparison, we plot the known gamut of *channel*- and *sphere*-type

quasi-ordered biophotonic nanostructures in bird feathers(*5*) (light gray shaded hulls), as well as insect, and engineered single gyroids and synthetic inverse opals at avian visible length scales (see also Fig. S2, and Table S1). The spectrum on the *x*-axes corresponds to the approximate avian-visible hue produced by a barb nanostructure of a given size (q_{pk}).

Figure 3. Evolutionary time-frozen snapshots of the disorder-order transition from ancestral, *channel*-type nanostructures with short-range order into derived single gyroid photonic crystals documented in a representative subset of *Chloropsis* species. SAXS diffraction patterns (Scale Bars - 0.05 nm^{-1}) of feather barbs from (**a**) iridescent green back of *C. cochinchinensis moluccensis*; (**b**) blue epaulette of *C. cochinchinensis kinabaluensis*; (**c**) turquoise blue throat of *C. jerdoni*; (**d**) blue malar stripe of *C. cyanopogon septentrionalis*; (**e**) blue coverts of *C. palawanensis*. (**a'-e'**) Azimuthal SAXS profiles corresponding the diffraction patterns in **a-e**, shown on a Porod background corrected (with a best-fit exponent of 3.5), normalized plot. The positions of fitted peaks are marked as shaded circles. (**a''-e''**) A hypothesized schematic (artistically rendered 2D sections starting from a model of spinodal decomposition in **e''**, courtesy of Tom Wanner), of the transition from mesoporous channel to single gyroid through a columnar intermediate with local nematic to hexatic order, informed by the SAXS data (**a-e**). (**f**) Barb biophotonic nanostructures of *Irena* and *Chloropsis* species exhibit a nearly linear increase in long-range periodic order with each additional higher-order peak observed in the azimuthal SAXS data.

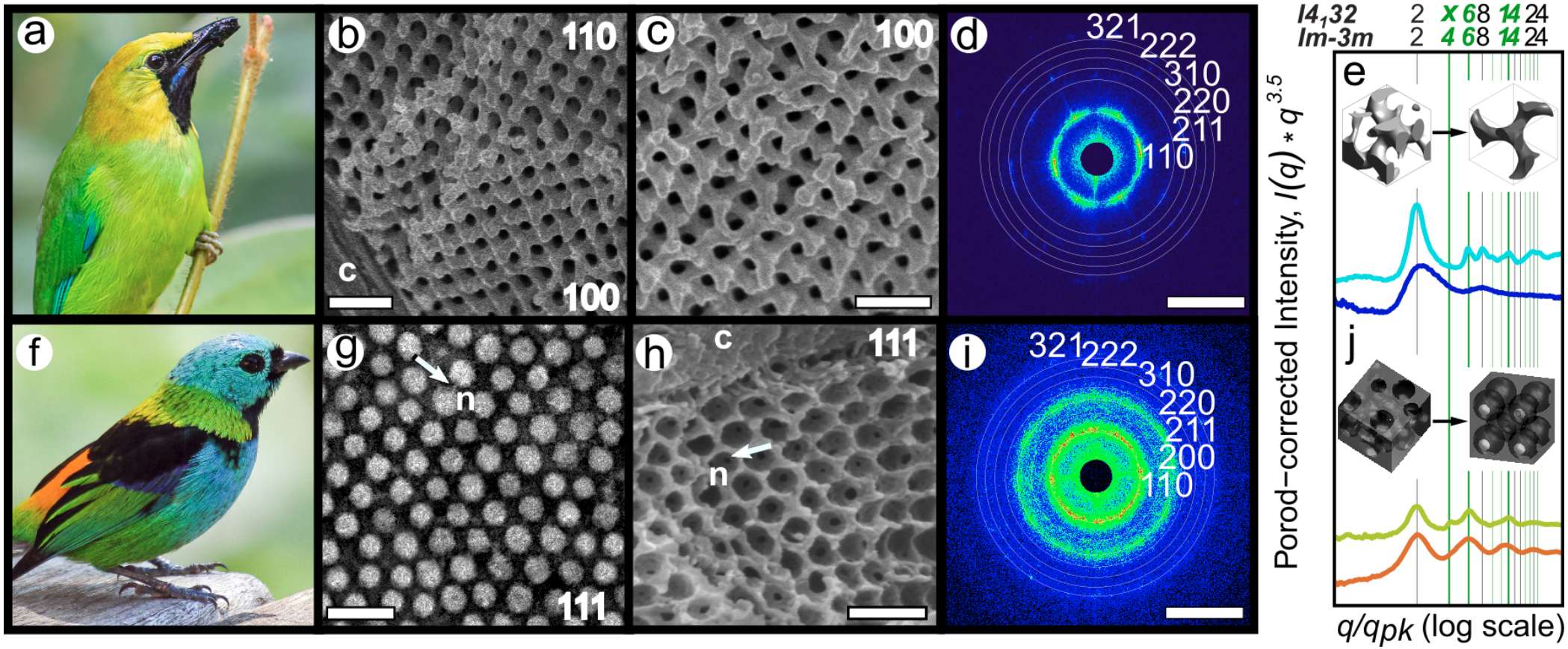
a
b
110
c
100
c
100
d
321
222
310
220
211
110
f
g
n
111
h
c
111
n
i
321
222
310
220
211
200
110
I4132
Im-3m
2 x 6 8 14 24
2 4 6 8 14 24
e
j
Porod−corrected Intensity, I(q) * q^3.5
q/qpk (log scale)

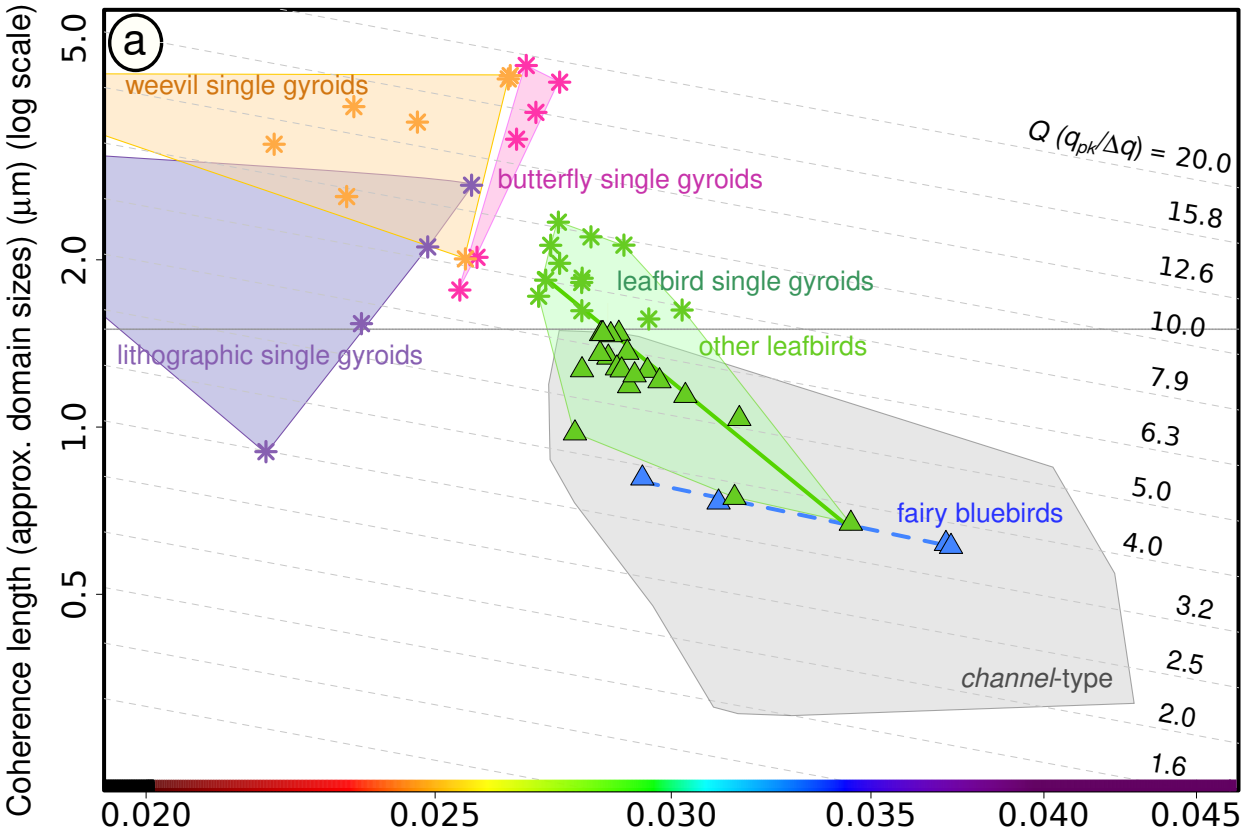
a
weevil single gyroids
butterfly single gyroids
leafbird single gyroids
other leafbirds
lithographic single gyroids
fairy bluebirds
channel-type
Q (qpk/Δq) = 20.0
15.8
12.6
10.0
7.9
6.3
5.0
4.0
3.2
2.5
2.0
1.6
Coherence length (approx. domain sizes) (µm) (log scale)
5.0
2.0
1.0
0.5
0.020
0.025
0.030
0.035
0.040
0.045

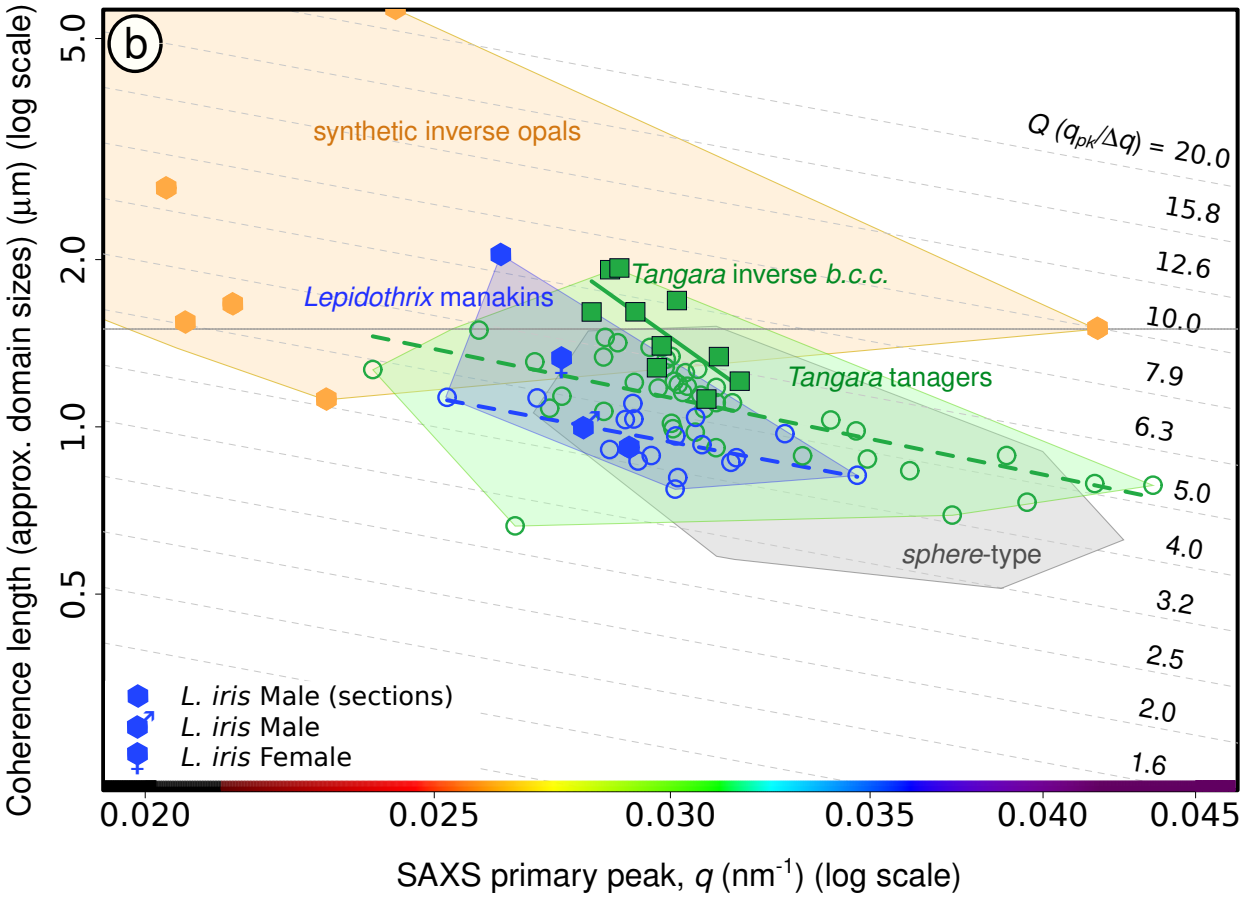
b
synthetic inverse opals
Lepidothrix manakins
Tangara inverse b.c.c.
Tangara tanagers
sphere-type
L. iris Male (sections)
L. iris Male
L. iris Female
Q (qpk/Δq) = 20.0
15.8
12.6
10.0
7.9
6.3
5.0
4.0
3.2
2.5
2.0
1.6
Coherence length (approx. domain sizes) (µm) (log scale)
5.0
2.0
1.0
0.5
0.020
0.025
0.030
0.035
0.040
0.045
SAXS primary peak, q (nm-1) (log scale)

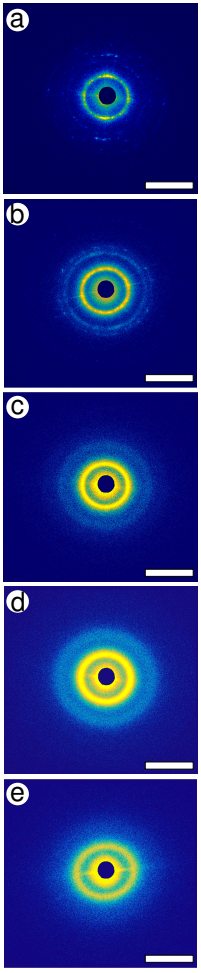
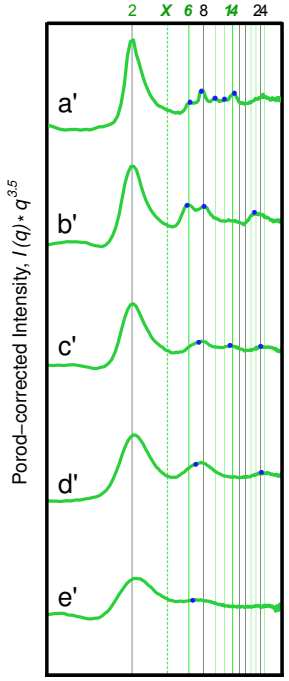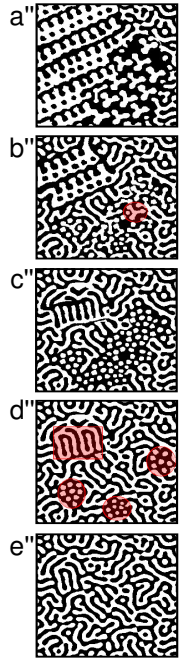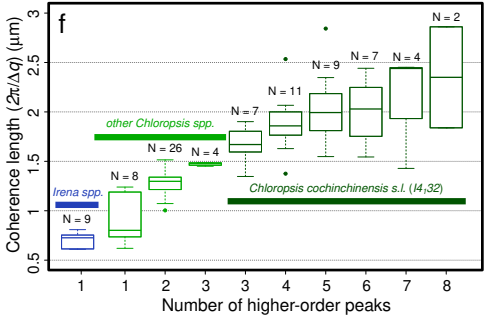
Increasing long-range periodic order